Assessment on the Effect of Sulfuric Acid Concentration on Physicochemical Properties of Sulfated-Titania Catalyst and Glycerol Acetylation Performance

Mohamad Rasid Shera Farisya [1] , **Ramli Irmawati [1,2,3,*]** , **Ishak Nor Shafizah [1,2]** , **Yun Hin Taufiq-Yap [1,2,4]** , **Ernee Noryana Muhamad [1,2,3]** , **Siew Ling Lee [5,6]** and **Nurrulhidayah Salamun [5]**

[1] Department of Chemistry, Faculty of Science, Universiti Putra Malaysia, Serdang 43400, Selangor, Malaysia; sherafarisya@gmail.com (M.R.S.F.); norshafizah@gmail.com (I.N.S.); taufiq@upm.edu.my (Y.H.T.-Y.); ernee@upm.edu.my (E.N.M.)

[2] Catalysis Science and Technology Research Centre (PutraCat), Faculty of Science, Universiti Putra Malaysia, Serdang 43400, Selangor, Malaysia

[3] Laboratory of Processing and Product Development, Institute of Plantation Studies, Universiti Putra Malaysia, Serdang 43400, Selangor, Malaysia

[4] Faculty of Science and Natural Resources, University Malaysia Sabah, Kota Kinabalu 88400, Sabah, Malaysia

[5] Department of Chemistry, Faculty of Science, Universiti Teknologi Malaysia, Johor Bahru 81310, Johor, Malaysia; lsling@utm.my (S.L.L.); nurrulhidayah@utm.my (N.S.)

[6] Centre for Sustainable Nanomaterials, Ibnu Sina Institute for Scientific & Industrial Research, Universiti Teknologi Malaysia, Johor Bahru 81310, Johor, Malaysia

* Correspondence: irmawati@upm.edu.my; Tel.:+60-3976-96786

Abstract: In this research, a solid acid catalyst was synthesized to catalyse glycerol acetylation into acetins. The sulphated-titania catalysts were prepared via the wet impregnation method at different sulfuric acid concentrations (5%, 10%, 15%, and 20%) and denoted as 5SA, 10SA, 15SA, and 20SA, respectively. The synthesized catalysts were characterized using FTIR, XRD, TGA, BET, NH_3-TPD, XRF, and SEM-EDX. The synthesized catalysts were tested on glycerol acetylation reaction at conditions: 0.5 g catalyst loading, 100–120 °C temperature, 1:6 glycerol/acetic acid molar ratios, and 2–4 h reaction time. The final product obtained was analysed using GC-FID. An increment in sulfuric acid concentration reduces the surface area, pore volume, and particles size. However, the increment has increased the number of active sites (Lewis acid) and strong acid strength. 15SA catalyst exhibited excellent glycerol conversion (>90%) and the highest selectivity of triacetin (42%). Besides sufficient surface area (1.9 m^2 g^{-1}) and good porosity structure, the great performance of the 15SA catalyst was attributed to its high acid site density (342.6 µmol g^{-1}) and the high active site of metal oxide (95%).

Keywords: glycerol acetylation; glycerol esterification; titanium dioxide; solid acid catalyst; triacetin

1. Introduction

Abundant glycerol generated in India is reported to be approximately 1.9 million litres as a by-product from the biodiesel industry. Glycerol is a by-product from the transesterification process of vegetable oil with straight-chain alcohol and produces fatty acid methyl ester (biodiesel) as the main product [1]. The surplus of glycerol waste has led to the search for an alternative approach, such as valorisation or conversion into valuable chemical products [2]. Several chemical transformation processes have been used for glycerol to improve its commercial availability and biodiesel economics. These processes are known as carboxylation [3], hydrogenolysis [4,5], selective oxidation [6], dehydration [7], oligomerization [8], etherification [9] and esterification or acetylation [10].

Among the derivatives of glycerol, acetins from glycerol acetylation reaction have received attention due to their use in a variety of products, such as food additives, medicine,

plasticizers, tanning agents, as well as their role as a monomer in the production of biodegradable polyester [11,12]. Triacetin has gained much attention recently as it is a high demanding product in fuel additives. The addition of 10% of triacetin in blended diesel–biodiesel can enhance engine performance, improve the anti-knocking properties, and, hence, reduce sNO_x/CO_x emissions [13]. The TA-based fuel additive has been proven to enhance fuel viscosity, cold flow, and thermal stability [14,15]. In general, the acetylation reaction of glycerol reacts with an acelating agent (acetic acid or acetic anhydride) and produces monoacetin (MA), diacetin (DA), and triacetin (TA), as shown in Figure 1 [16,17]. Acetylation reaction with acetic acid is an endothermic reaction that needs high energy in order to achieve a high yield of TA. Meanwhile, the exothermic reaction of acetic anhydride introduces a third acetyl group favouring TA formation [18]. Due to the corrosive nature of acetic anhydride, acetic acid is preferable as it is an organic compound and is less harmful to the environment [19,20]. Nonetheless, many reported works have produced low TA selectivity [21–23]. The utilization of catalysts in glycerol acetylation is a promising approach. However, achieving high TA selectivity is still a crucial part of glycerol acetylation.
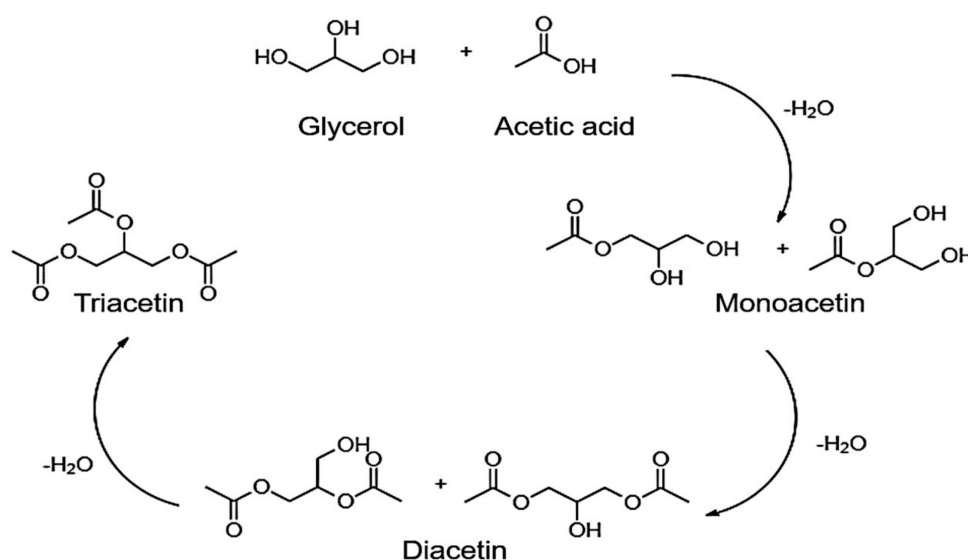
Figure 1. Reaction pathway of acetylation of glycerol with acetic acid.

Commonly, sulfuric acid, p-toluene sulfonic acid, hydrofluoric acid, and acid ionic liquid are used as homogenous catalysts in glycerol acetylation [24,25]. According to Nda-Umar et al. [26], the use of strong acid catalysts has been demonstrated to improve the performance of glycerol acetylation. However, the acid catalysts mentioned above are known as homogenous catalysts, which take the form of liquid. As a result, they suffer from various drawbacks, such as high energy consumption, they are not reusable, they have a complex separation process, and the cost of the purification process is high. Moreover, the huge amount of wastewater generated could harm the environment [27,28]. Recent studies have worked towards the improvement of heterogeneous catalysts in order to circumvent these problems [26]. Among the reported works are the development of an ion exchange resin [29,30], supported heteropolyacids [31], mesoporous silica [32], zeolite [33], montmorillonite [34] enzyme [35] and metal oxide [10] catalysts. The solid nature of these catalysts are able to overcome the drawbacks of homogeneous catalysts and, as a result, product-catalyst separation becomes less complex, catalyst recovery is easier, it becomes reusable and regenerable, and it produces less waste sludge and wastewater, hence reducing operation cost and energy consumption. To date, carbon-based catalysts have shown an excellent performance in glycerol acetylation, with 57% TA selectivity and 86% glycerol conversion. This was reported by Nda-Usman et al. [36], who performed a glycerol acetylation reaction at an operating condition of 1:6 *w/v* of glycerol: acetic acid

molar ratio (5 g glycerol and 18.6 mL acetic acid), with 0.5 g sulfonated carbon catalyst at a 450 rpm of stirring rate, which could be used as a reference for any catalytic trial in the preliminary stage. Besides carbon catalysts, metal and metal oxides catalysts have also demonstrated great performance in glycerol acetylation due to their high thermal stability and are active in a wide range of the temperatures [37]. Almas et al. [38] worked on a zirconia catalyst in glycerol acetylation and produced very low TA selectivity (0.2%). Ramalingam et al. [39] investigated glycerol acetylation using Ag-Cu bimetallic doped on a rice husk silica-alumina catalyst and obtained 38% TA selectivity with 98% glycerol conversion. They performed at operating conditions of 0.8 g catalyst loading, 1:10 w/v ratio of glycerol to acetic acid at 110 °C.

Appaturi et al. [14] synthesized the nickel supported titania catalyst via the simple sol–gel method with different amounts of Ni^{2+} (0%, 10%, 30%, and 50%) supported on the surface of titania ($nNiO/TiO_2$). The glycerol acetylation reaction was conducted using a 1:10 mole ratio of glycerol to acetic acid, 150 °C for 15 min using a non-microwave instant heating technology (Monowave 50, Anton Paar, Subang Jaya, Selangor, Malaysia). They found that $30NiO/TiO_2$ catalysts show an outstanding performance in glycerol acetylation with 90% glycerol conversion and 65% TA selectivity. This was attributed to the $30NiO/TiO_2$ catalysts properties, which have a larger particle size (126 ± 26 nm), high total acid sites (1228 μmol g^{-1}), and high accessible surface area of the catalyst (79 m^2 g^{-1}). However, conventional heating techniques are still preferable in glycerol acetylation compared to microwave heating, which might face a challenge in upscale production due to the uncontrollable heating processes and low penetration depth in the reactive media [40].

On the other hand, Kulkarni et al. [10] stated that the substitution of a sulphate group in metal oxide catalyst development boosted the catalytic performance in glycerol acetylation. The presence of the sulphate group on the catalyst surface increased the availability of the active sites. They also reported that SO_4^{2-}/CeO_2-ZrO_2 catalyst achieved high TA selectivity compared to the non-sulphated CeO_2-ZrO_2 catalyst, with 21% and 0.5% TA selectivity, respectively. They reported that the characteristics of SO_4^{2-}/CeO_2-ZrO_2 catalyst has high acid site density (2.5 mmol), sufficient space of BET surface area (22 m^2 g^{-1}) good pore diameter (5.9 nm) for reaction to occur. Rane et al. [41] found sulphated-alumina has higher TA selectivity (23% TA selectivity) compared to metal-supported with non-sulphated-alumina (0.5% TA selectivity). This activity of the catalysts tested corresponded to the number of acid sites density. They stated that a sulphated-alumina catalyst is higher compared to a non-sulphated catalyst with 2.5 mmol and 1.2 mmol, respectively.

In this study, sulphated titania was synthesized via the impregnation method. The incorporation of sulphate group onto a titania catalyst might enhance the catalytic performance in glycerol acetylation. Sulfated-titania has never been reported in glycerol acetylation. Sulphated titania has never been reported in glycerol acetylation. However, Tomer and Biswas [42] prepared sulphated-titania catalyst for a different application, which is the dehydration of fructose to 5-hydroxymethylfurfural (5-HMF). The 0.5 M SO_4^{2-}/TiO_2 catalyst showed excellent catalytic activity and successfully yielded 75% of 5-HMF (main product). The catalyst has a high acid site density (0.6 mmol g^{-1}) and surface area (25 m^2 g^{-1}), resulting in a higher yield of 5-HMF.

Geetha et al. [43] examined the performance of sulphated-titania catalyst via pseudo-five-component reaction. They found that the sulphated-titania obtained a higher yield (90%) of functionalizing piperidine compared to non-sulphated-titania (48%). The acid site properties of sulphated catalysts play a vital role in catalytic activity. The presence of Bronsted and Lewis acid sites might help enhance the glycerol acetylation in this study.

In this study, glycerol acetylation reaction is performed by using a newly synthesized catalyst, sulphated titania. The sulphated-titania catalyst was prepared using the wet impregnation method by varying the sulfuric acid concentration at 5%, 10%, 15%, and 20%. Following previously reported works, the TA selectivity remained low in the presence of the metal oxide catalyst. Meanwhile, the incorporation of sulphate groups on metal

oxide catalysts has boosted catalytic activity. Herein, the main interest of this study is to acquire high TA selectivity with optimum characteristics of the sulphated-titania catalyst. The effect of the sulfuric acid concentration on the catalyst properties and TA selectivity were studied.

2. Results and Discussion

2.1. Physicochemical Properties of the Synthesized Catalyst

Figure 2 shows the FTIR spectra of all synthesized catalysts. The FTIR analysis was performed to confirm the presence of the sulphate group in the sulphated-titania catalyst and to evaluate the effect of sulfuric acid concentration on the band properties for each functional group of the synthesized catalyst. For sulphated catalysts (5SA, 10SA, 15SA, and 20SA), strong broadband between 3600 cm^{-1} and 3000 cm^{-1} is assigned to O–H stretching in H-bonded water. The chemical and physical absorption of the hydroxyl group on the surface of the sulphated catalysts proves that these catalysts are anhydrous metal oxide catalysts [44,45]. The band observed at 1632 cm^{-1} is due to the scissor bending vibration of the molecular water (H–O–H), assigned as chemisorbed water [46,47]. A band between 1222 cm^{-1} to 1100 cm^{-1} are assigned to the S=O group which indicates the existence of sulphate species. Besides, the bands between 1057 and 994 cm^{-1} was attributed to symmetry and asymmetry stretching of the S-O bond [17,48] has obtained a similar observation, where the S-O bands are assigned to chelating bidentate SO_4^{2-} in coordination with Ti^{4+} metal. Therefore, the experimental result of the FTIR spectrum shows that the relative functional group present in synthesized catalysts indicates the sulfation has successfully occurred in this study.
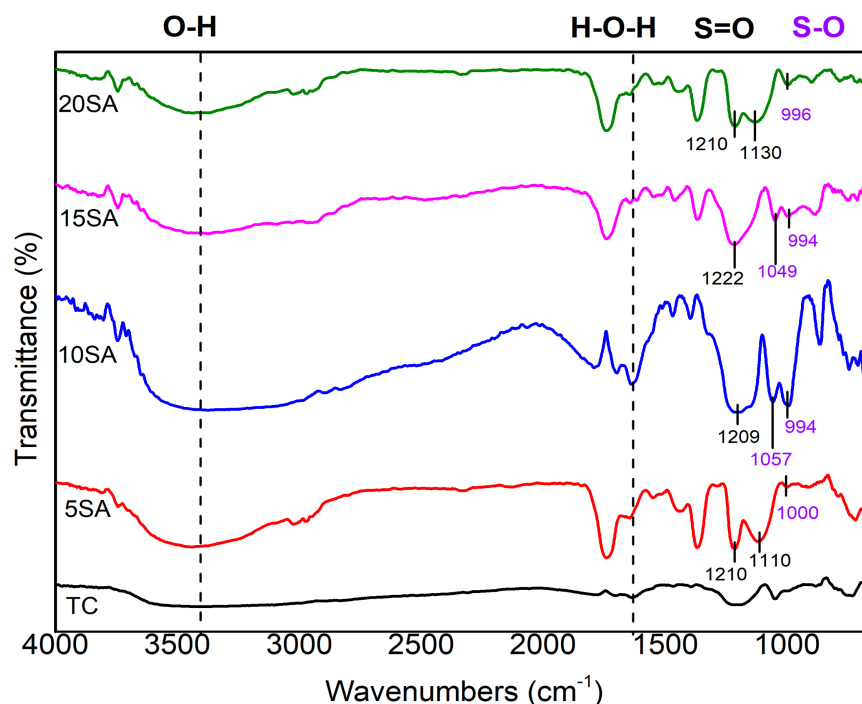
Figure 2. FTIR spectra of non-sulphated and sulphated-titania catalysts at various concentration.

The XRD profile of non-sulphated (TC) and sulphated-titania with different concentrations of sulfuric acid (5SA, 10SA, 15SA, and 20SA) are displayed in Figure 3. The diffraction peaks of TC were detected at 2θ = 25.3°, 37.0°, 37.9°, 38.7°, 54.0°, 55.1°, 58.1°, 62.7°, 68.8°, 70.3°, 75.1°, 76.1°. These peaks correspond to the anatase phase according to JCPS: 96-900-8214 with the chemical formula of Ti_4O_8. TC has a single phase of TiO_2 anatase (100%) with a tetragonal structure. This finding is similar to Dabbawala et al. [49]. On the other hand, the diffraction peak for 5SA, 10SA, 15SA, and 20SA catalysts, new

peaks observed at $2\theta = 25.3°, 37.0°, 37.9°, 55.1°, 62.7°, 68.8°, 70.3°, 76.1°$ corresponds to $(TiO)(SO_4)(H_2O)$ with an orthorhombic structure. Referring to the X'Pert HighScore Plus software, the hkl plane changed for non-sulphated and sulphated-titania from 1,0,1 planes to 2,1,0 planes, aligning with the changes in catalyst structure. The chemical formula for all sulphated-titania catalysts is $O_{24}Ti_4S_4$ with an orthorhombic structure. The increment in sulphate concentration for sulphated-titania impacted the crystallinity of $(TiO)(SO_4)(H_2O)$ at the peak of 25.3°. The intensity of the peak reduced and broadened as the concentration of sulfuric acid increased. The sulphated catalysts became amorphous material as more sulfuric is loaded onto titania. This finding is in agreement with Yang et al. [50]. They mentioned that the reduction of peak intensity is probably due to the partially dissolved TiO_2 in H_2SO_4 during the sulfation of the catalyst. The crystallite sizes are tabulated in Table 1. The particle size of TC is the highest compared to 5SA, 10SA, 15SA, and 20SA with 80 nm, 64 nm, 67 nm, 36 nm, and 44 nm, respectively. Increasing the sulphate concentration decreases the particle size and aligns with results from Oliveira et al. [51].
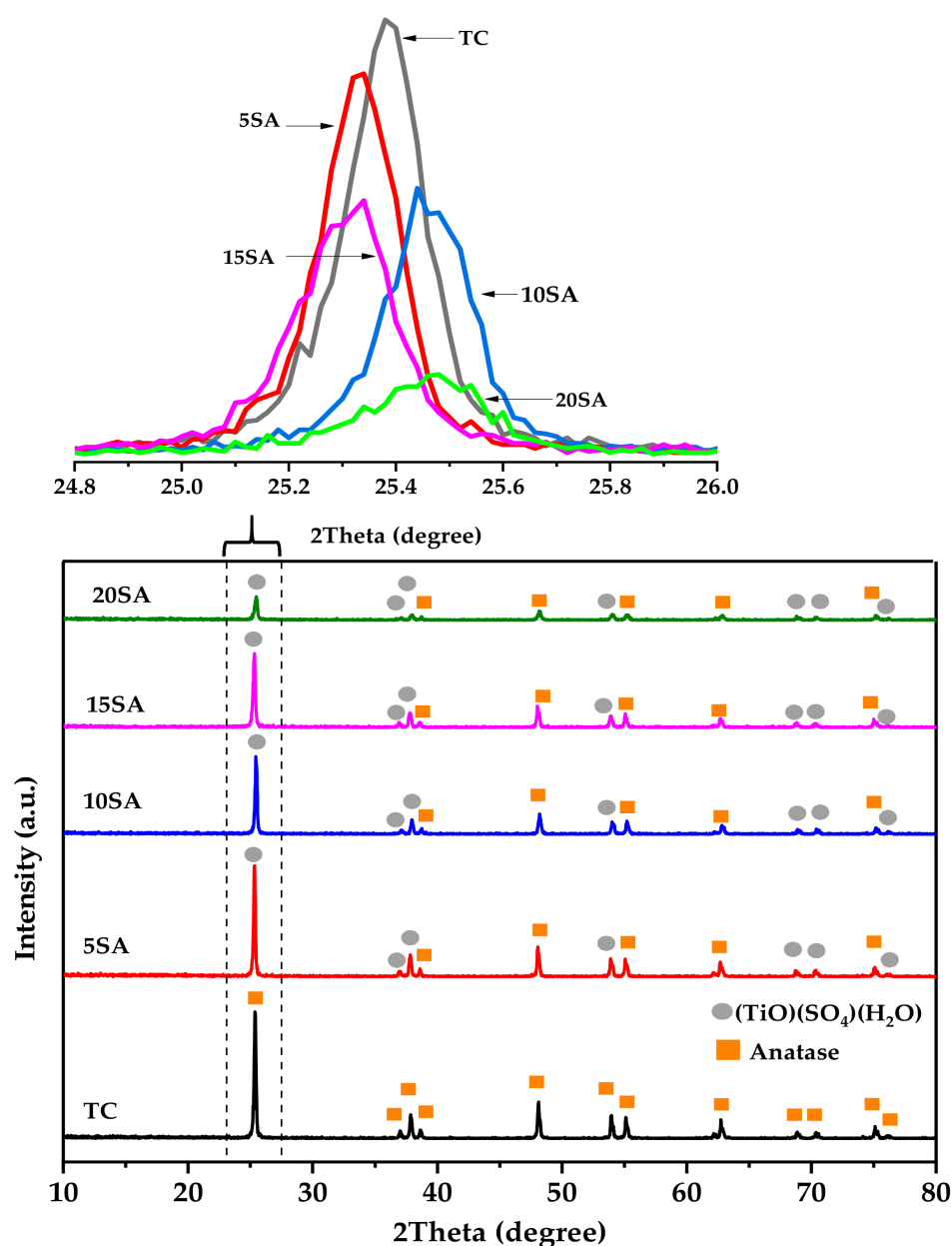
Figure 3. XRD profile of non-sulphated and sulphated-titania catalysts at various concentration.

The TGA-DTG curve of non-sulphated (TC) and sulphated-titania catalyst (5SA, 10SA, 15SA, and 20SA) was shown in Figure 4. The thermal stability and decomposition of the synthesized samples were evaluated within the range of 50–1000 °C. For TC, a minor weight loss at temperature <200 °C due to loss of hydrate compound presence in TC was observed. Dabbawala et al. [49] and Deris et al. [52] also found that the moisture or water molecule decomposition occurs at a lower temperature (<200 °C). As mentioned in the XRD results, the sulphated-titania catalysts are anhydrous metal oxide catalysts. The first weight loss for sulphated-titania catalyst also detected at the same temperature range could be due to the decomposition of physisorbed and chemisorb water molecules on the catalyst structure. As observed in Figure 4, the weight loss of water molecules for 20SA is higher than 15SA, 10SA, and 5SA. This is probably due to 20SA having the highest hydrophilicity properties compared to other sulphated catalysts [53]. The second weight loss observed at the temperature between 300 and 700 °C represents sulphate decomposition. Among sulphated-titania catalysts, the loss of sulphate group for 5SA occurred at the lowest region (300–600 °C) followed by 10SA (450–650 °C), 15SA and 20SA (500–750 °C). DTG curve also shows that the weight loss at maximum temperature for sulphated titania shifted gradually towards a higher temperature region accordingly. This indicates that sulphate species for 5SA has the weakest bond on the surface of the catalyst. The third weight loss appeared only for 10SA, 15SA, and 20SA catalysts. The weight loss percentage at a temperature range of 850–950 °C is minimal $1 \pm 0.5\%$ for 10SA and $2 \pm 0.5\%$ for both 15SA and 20SA. This indicates that the high sulphate concentration has strengthened the sulphate intermolecular bond and may require more heat to undergo the sulphur group of decomposition. This finding is in agreement with Liu et al. [53]. At a higher temperature, SO_4^{2-} in the sulphated sample will escape in the form of SO_2.
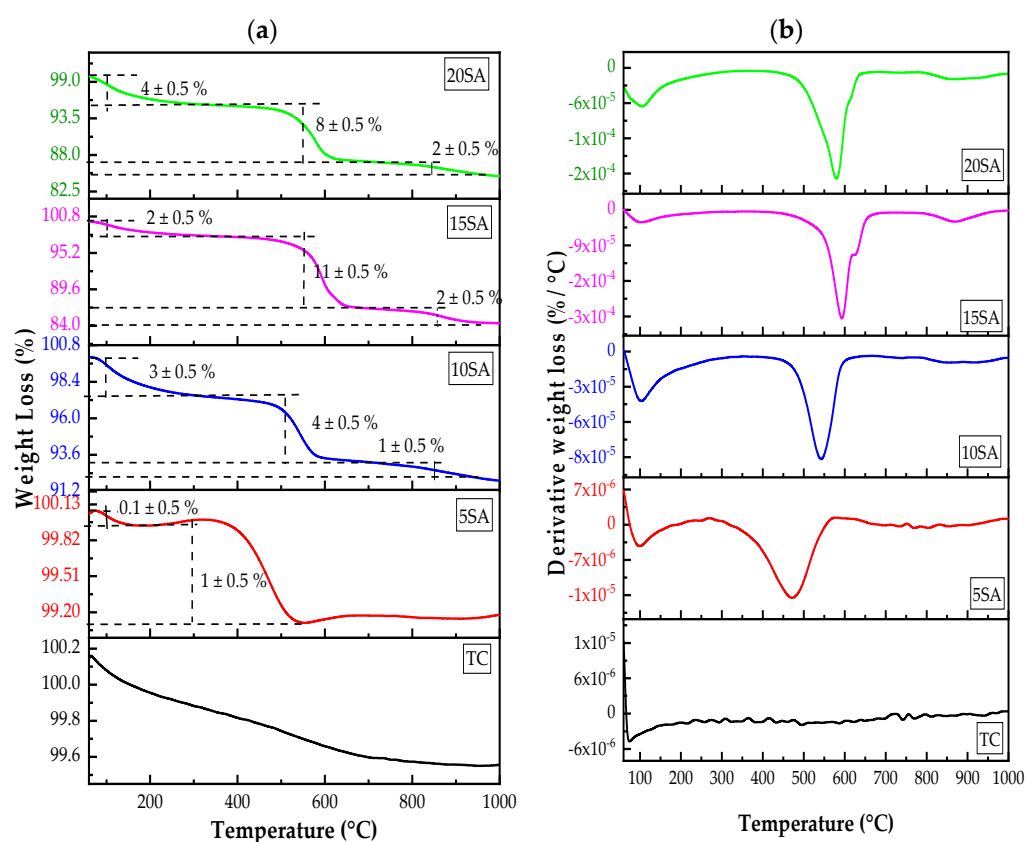
Figure 4. TGA (**a**) DTG (**b**) curve of non-sulphated and sulphated−titania catalysts at various concentration.

Information regarding BET surface area, pore volume, and pore diameter of the catalyst are tabulated in Table 1. TC has the highest surface area with 11.8 m² g⁻¹. For the 5SA catalyst, the surface area decreases to 7.4 m² g⁻¹ as the sulphate group is incorporated into the titania surface, which leads to the formation of titanium sulphate. Nevertheless, increasing the sulfuric acid concentration decreases the surface area to 6.2 m² g⁻¹, 1.9 m² g⁻¹, 0.2 m² g⁻¹, for 10SA, 15SA, and 20SA, respectively. The decrement in the surface area for sulphated catalysts might be due to the aggregation of a small titania sulphate particle on the titania oxide surface and the plugging of the larger pores by the sulphate species might have occurred [42]. The average pore volume also shows the same trend. This will contribute to the reduction in pore volume. A similar trend is shown for pore volume values in Table 1 when sulfuric acid concentration increases. Further pore blockage might have occurred due to the agglomeration of sulphate particles. In addition, the pore diameter of the non-sulphated and sulphated catalyst within the range of 5.4 nm to 5.2 nm, which is capable of accommodating the glycerol molecule (1 nm) for the reaction to occur on the pore surface.

Table 1. The BET surface area and porosity of non-sulphated and sulphated-titania catalysts at various concentration.

Catalyst	BET Surface Area (m² g⁻¹)	Pore Volume (nm)	Pore Diameter (nm)
TC	11.8	0.0029	5.4
5SA	7.4	0.0016	5.4
10SA	6.2	0.0014	5.2
15SA	1.9	0.0003	5.2
20SA	0.2	0.00003	5.2

The main element in the non-sulphated and sulphated-titania catalysts was identified via X-ray fluorescence analysis (XRF). According to Table 2, the major chemical composition of sulphated catalysts is TiO_2 and SO_3. Only TiO_2 composition is detected in the non-sulphated catalysts. All synthesized catalysts have the highest value of TiO_2 in the range of 90–99%. A trace amount of SO_3 was detected for all sulphated catalysts in the range of 1–10%. Herein, the presence of sulphate confirms that the sulphate species was successfully impregnated on the titania surface.

Table 2. The elemental analysis and surface acid distribution of non-sulphated and sulphated catalyst.

Catalyst	XRF Analysis		NH₃-TPD Analysis
	TiO₂ (%)	SO₃ (%)	Amount of NH₃ Adsorbed (µmol g⁻¹) *
TC	99	-	12.9
5SA	99	1	28.1
10SA	95	5	279.0
15SA	95	5	342.6
20SA	90	10	444.6

* The amount of NH_3 adsorbed from the sample is referred as total acid sites density.

The NH_3-TPD profiles of non-sulphated and sulphated-titania catalysts are displayed in Table 2 and Figure 5. The desorption peaks were recorded at two different regions indicating the presence of weak acid sites (T_{max} =< 250 °C) and strong acid sites (T_{max} => 500 °C). Meanwhile, the desorption peak of sulphated-titania catalyst appeared at T_{max} more than 500 °C. As can be seen in Figure 5, TPD profiles of 10SA, 15SA, and 20SA catalysts were observed at the high-temperature region at 579 °C, 608 °C, and 600 °C, respectively. It shows that strong acid sites are present on the sulphated-titania catalyst surface. The weak acid sites are related to the Bronsted acid site of Ti-OH, while the stronger acid site stands for the Lewis acid centre [50]. As the sulfuric acid concentration increases, the peak shifted

towards a higher temperature. It may be due to the increased number of the amount of NH_3 adsorbed (Table 2) by catalyst which indicates the higher total acids sites density of sulphated-titania catalyst. The larger the desorption peak temperature due to the higher number of active sites. Increases in the sulfuric acid concentration increased the availability of active sites on sulphated-titania catalysts. From this observation, the sulphation of the titania may create more Lewis acid sites and strengthen the acidity strength, hence enhancing glycerol conversion and TA selectivity.
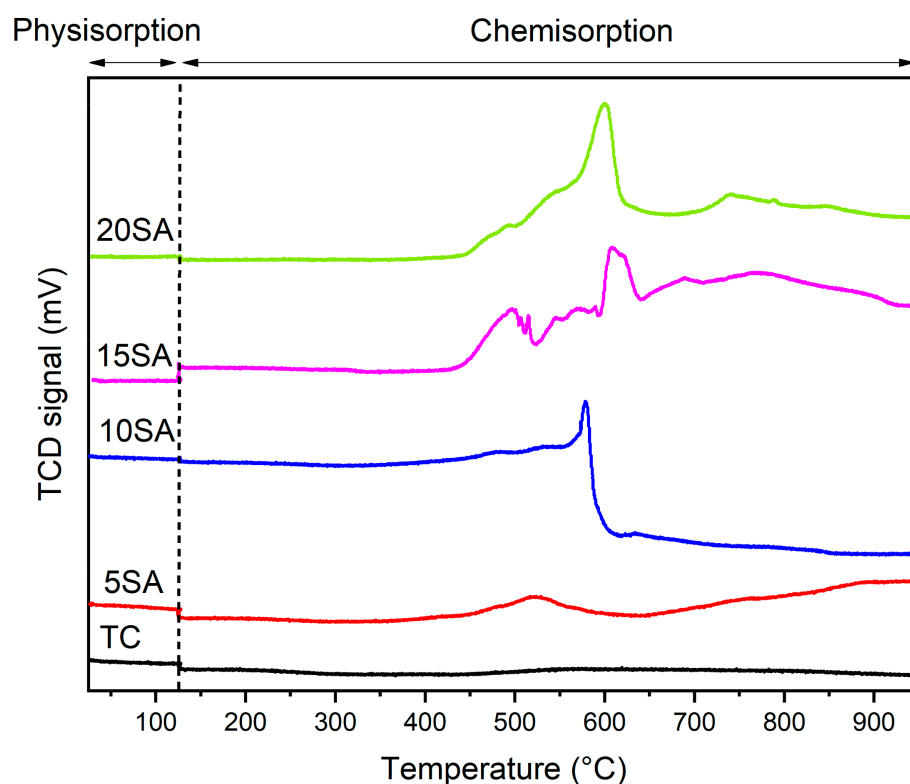
Figure 5. NH_3-TPD profile of non-sulphated and sulphated-titania catalyst at various concentration.

SEM-EDX analysis was used to study the surface morphology and elemental composition of non-sulphated and sulphated-titania catalysts. According to the SEM micrograph in Figure 6, TC shows uniform distribution of spherical particles. From EDX analysis, two peaks detected corresponds to titania and oxygen at 0.5 keV and 0.6 keV, respectively. As can be seen in Figure 6, the morphology for all sulphated catalysts display a nearly spherical shape with a crumb-like structure due to particle agglomeration. However, the EDX analysis clearly shows that all expected elements are present. The elemental compositions present in the sulphated-titania catalysts are titania (Ti), oxygen (O), and sulphur (S). The peak detected Ti, O, and S at 0.5 keV, 0.6 keV, and 2.3 keV, respectively. Hence, the additional peak of S confirmed that the sulfation was successfully impregnated on the Ti surface. This finding is similar to Liu et al. [53]. Besides, the intensity peak of sulphur increased as the sulfuric acid concentration increased. This finding correlates with XRF and NH_3-TPD analysis. The number of sulphate and active sites increases according to the increment in sulfuric acid concentration.
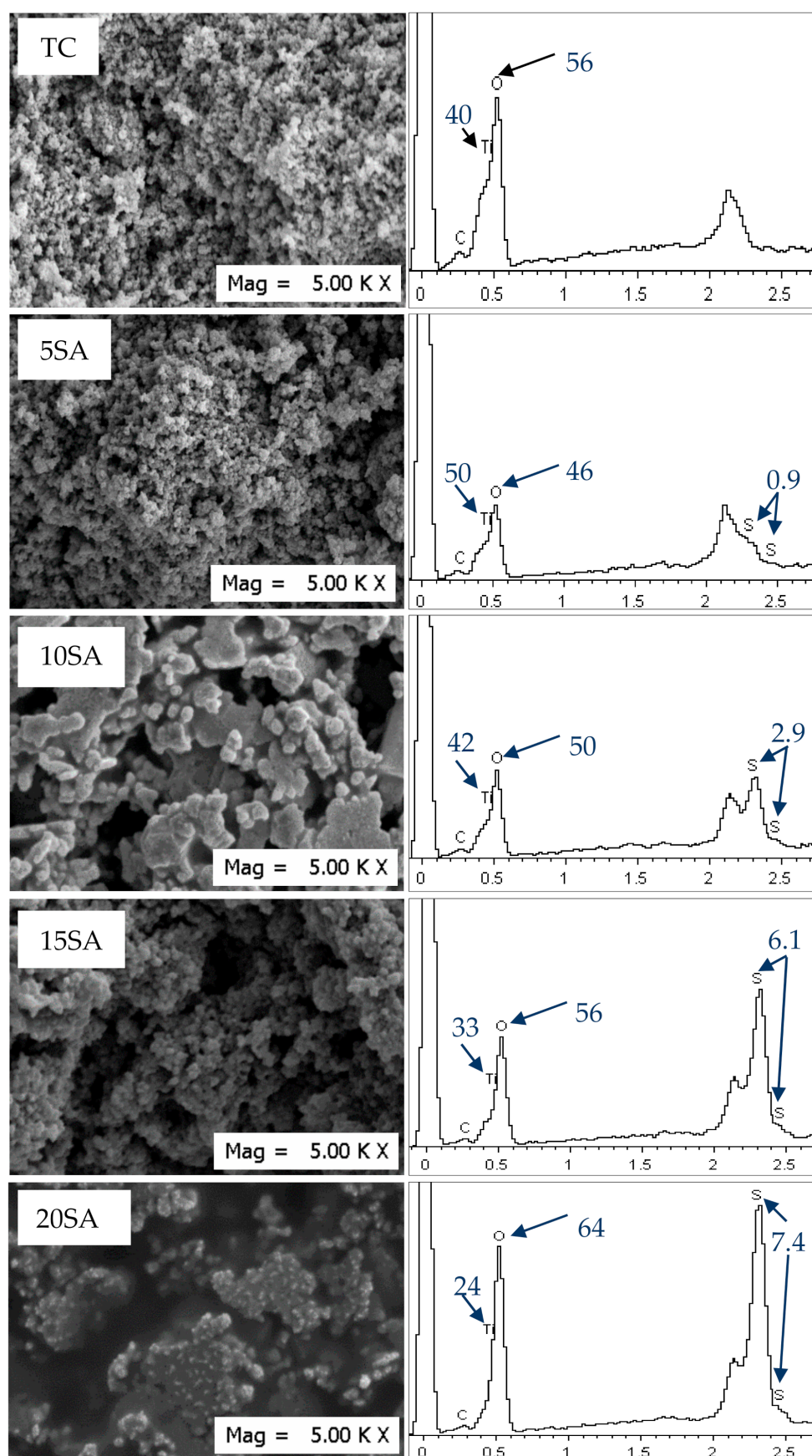
Figure 6. SEM micrograph of sulphated and uninsulated titania catalyst.

2.2. Catalytic Performance in Glycerol Acetylation

The glycerol acetylation was performed at an operating condition temperature of 100–120 °C, 0.5 g of catalyst loading, and glycerol: acetic acid mole ratio of 1:6. This study was carried out to find an outstanding sulphated-titania catalyst in producing the highest TA selectivity. Figure 7 displays the glycerol conversion and MA, DA, and TA selectivity for blank, TC, 5SA, 10SA, 15SA, and 20SA. A blank reaction is a reaction that was conducted without a catalyst. As can be seen in Figure 7, for blank reaction, the 58% glycerol was converted into acetins (51% MA, 22% DA, and 1% TA). The acetic acid can act as a self-catalysing effect and could drive the reaction forward due to its acidic nature. This finding was similar to Nda-Umar et al. [26]. Moreover, the glycerol conversion was significantly increased when using non-sulphated titania (TC) up to 100%. The composition of acetins achieved was 22% MA, 63% DA, 16% TA. Even though the active acid sites for TC is lower (12.9 μmol g^{-1}), it is sufficient to allow the reaction to happen. The high surface area (11.8 m^2 g^{-1}) and sufficient pore volume (0.0003 cm^3 g^{-1}) and pore diameter (5.4 nm) could contribute to the TA formation. The results on glycerol conversion for sulphated-titania catalyst at different sulfuric acid concentrations are showing a trend. Increasing the sulfuric acid concentration decreases the glycerol conversion. According to Figure 7, the highest TA selectivity was obtained at 15SA (42%), followed by 10SA (41%), 5SA (38%), and 20SA (36%), respectively. These findings aligned with the physicochemical properties of the synthesized sulphated titania at different concentrations. Even though the TA selectivity for each catalyst shows a small difference, especially for 10SA and 15SA. The 15SA catalyst has been chosen as the best catalyst for glycerol acetylation. The catalyst produced the highest TA selectivity owing to its higher acid sites density (342.6 μmol g^{-1}) as compared to 10SA. The TA selectivity for 20SA was lower, even though the acid sites density was higher (444.6 μmol g^{-1}). This may be due to its lower surface area (0.2 m^2 g^{-1}), pore volume (0.00003 cm^3 g^{-1}), and pore diameter (5.2 nm). The triacetin molecule requires sufficient space to form.
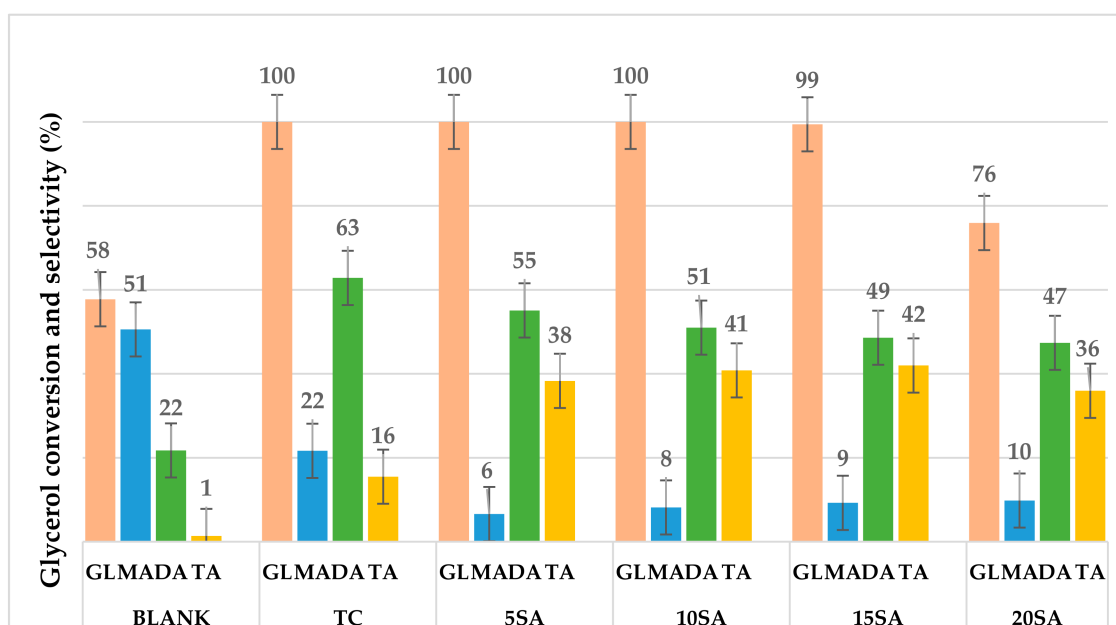
Figure 7. The glycerol conversion and product selectivity. Reaction condition: 1:6 *w/v* glycerol: acetic acid mole ratio (5 g glycerol, 18.6 mL acetic acid) 0.5 g catalyst loading, 100–120 °C, 2–4 h, 450 rpm. GL: Glycerol conversion, MA: Monoacetin, DA: Diacetin, TA: Triacetin.

2.3. Catalytic Comparative Study

In this section, the comparison of the performance of the synthesized catalysts with other metal oxide catalysts reported was evaluated. Table 3 summarized all the catalysts according to their synthesis technique, the type of acelating agent used and reaction parameters. Based on this study, 15SA is the best catalyst, producing the high glycerol conversion (99%) and TA selectivity (42%). As presented in Table 3, there are three Ti-based catalysts selected for comparison study, which are $30NiO/TiO_2$, $Fe-Sn-Ti(SO_4^{2-})$-400, and MoO_x/TiO_2-ZrO_2. All the catalysts show high glycerol conversion in the range of 90% to 100%. Among the three catalysts, $Fe-Sn-Ti(SO_4^{2-})$-400 catalyst shows the highest TA selectivity (99%). The utilization of acetic anhydride and multi-metal acid catalyst might help in producing more TA yields. However, the use of acetic anhydride may be less practical on a large scale because it is expensive and may cause an explosion due to being highly exothermic. On the other hand, $30NiO/TiO_2$ catalyst achieved 66% TA selectivity under the non-microwave instant method. The microwave is proven the best technique in speeding up the reaction process with a higher yield product. Nonetheless, the temperature is quite high as compared to other reported works. High energy consumption might increase the overall cost of production when upscaling the process. On the contrary, MoO_x/TiO_2-ZrO_2 catalyst shows a low TA selectivity (8%) where the monoacetin is the major product (52%). The glycerol acetylation using sulphated titania prepared via impregnation method and using less harmful organic acid (acetic acid) could be the alternative process in the future. However, this study must be continued in finding the optimum condition for glycerol acetylation. 15SA catalyst could be great potential because this catalyst can be prepared using a simple method, less chemical and solvent used, and require mild conditions in production, low energy consumption, and low-cost production.

Table 3. Comparative study on glycerol acetylation using titania catalysts and method.

Catalyst	Method	AA	Reaction Parameters				GL (%)	Selectivity (%)			Ref.
			T (°C)	MR	CL (g)	t (h)		MA	DA	TA	
Blank	Reflux	AAC	100	1:6	-	2	58	51	22	1	This work
TC (Non sulfated titania)	Reflux	AAC	100	1:6	0.5	2	100	22	63	16	This work
5SA (sulfated titania)	Reflux	AAC	100	1:6	0.5	2	100	7	55	38	This work
10SA (sulfated titania)	Reflux	AAC	100	1:6	0.5	2	100	8	51	41	This work
15SA (sulfated titania)	Reflux	AAC	100	1:6	0.5	2	99	9	49	42	This work
20SA (sulfated titania)	Reflux	AAC	100	1:6	0.5	2	76	10	47	36	This work
$30NiO/TiO_2$	Non-Microwave instant	AAC	170	1:10	0.04	0.5	90	20	15	66	[14]
Fe-Sn-Ti (SO_4^{2-})-400	Autoclave	AAH	80	Gly-1.5 g, AAH-8.4g	0.05	0.5	100	0	1	99	[17]
$MoOx/TiO_2$-ZrO_2	Reflux	AAC	120	1:6	5 wt%	3	100	52	41	8	[54]

AA = Acelating agent (AAC = Acetic acid, AAH = Acetic anhydride), T = Temperature, MR = Mole ratio, CL = Catalyst loading, t = Time, Gly = Glycerol, GL = Glycerol conversion, MA = Monoacetin, DA = Diacetin, TA = Triacetin, Ref = References. (The highlighted rows are the main finding in this work in comparison with other related work in getting higher TA selectivity).

3. Materials and Method

3.1. Materials

Anhydrous glycerol (99%), sulfuric acid (95–98%) and glacial acetic acid (99%) were purchased from R&M Chemicals, Ltd., Subang, Malaysia. Titanium dioxide (98%), acetonitrile (GC grade) and 1,3-butanediol were purchased from Sigma-Aldrich, St. Louis, MO, USA. All chemicals obtained were used without further purification.

3.2. Catalyst Preparation

The sulphated-titania oxide catalysts were prepared through the impregnation method as shown in Figure 8. Firstly, TiO_2 was soaked in the 5 v/v% sulfuric acid solution for 24 h at room temperature. The sulphated-titania was dried overnight in an oven at a temperature of 100–120 °C. After that, the dried sulphated titania was ground and sieved using a mesh sieve (350 µm). The sample was then calcined in a tabular furnace at a temperature of 400–500 °C for 2–4 h under a CO_2 environment. The synthesized catalyst was labelled as 5SA. The procedures were repeated similarly but at various concentrations and the prepared samples were denoted as xSA, where x attributed to sulfuric acid concentration (10, 15 and 20%). Non-sulphated titania catalyst was also prepared as a precursor without adding sulfuric acid into the titania and denoted as TC.
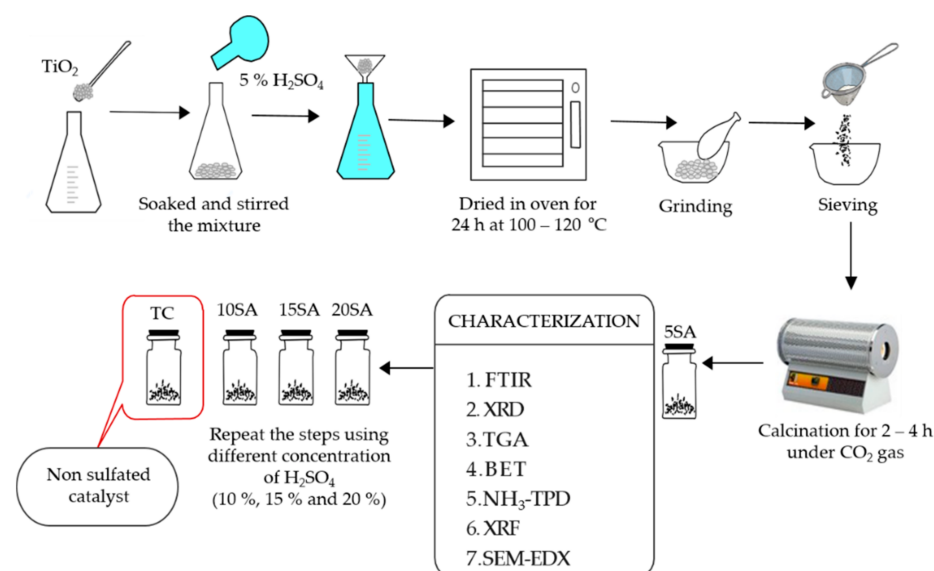
Figure 8. Preparation of non-sulphated and sulphated-titania catalyst at various concentration.

3.3. Catalyst Characterization

The crystalline phases of non-sulphated and sulphated-titania catalysts were determined by an X-Ray diffractometer with Shimadzu model XRD 6000 (Shimadzu Malaysia Sdn. Bhd., Petaling Jaya, Selangor, Malaysia). The sample was put on the sample disc and placed in the path of the X-Ray beam. After that, the cathode ray tube will generate the X-rays by heating the filament to accelerate and direct the electron towards the samples (Cu K_α radiation source of 30 kW and electricity of 30 Ma). The X-rays will interact with the sample producing constructive interference and diffracted rays. The sample and the detector were rotated through a scanning range of 2θ = 10–80°, scanning speed of 4° min^{-1} and wavelength (λ) of 1.54 Å. Lastly, the diffraction pattern of the synthesized catalyst generated was recorded. The crystallite sizes were calculated using Debye-Scherrer's formula equation, where D_{hkl} corresponds to the average crystallographic size in the h,k,l direction, K is the crystallite-shape factor, λ is the wavelength of incident X-ray, β is the X-ray diffraction broadening (Full Width at Half-Maximum–FWHM, in radians), and θ is the angle between the incident rays and the surface of the materials (Bragg angle).

The functional group of the synthesized catalysts was evaluated using Fourier transform infrared spectroscopy—FTIR) by Perkin Elmer, 1650 Spectrometer (Petaling Jaya, Selangor, Malaysia). The sample was placed in the sample holder and inserted into the instrument with the spectroscopic range of 650 cm^{-1} to 4000 cm^{-1}. The absorption frequency was recorded as percentage transmittance against wavenumber.

A Mettler Toledo 851e (Im Langacher, Greifensee, Switzerland) Switzerland thermal analysis instrument was used to determine the thermal stability of the synthesized catalysts. In this study, the samples were placed on the sample pan inside the instrument furnace and heated from 50 to 900 °C under a continuous flow of nitrogen gas (N_2) at 50 mL min^{-1} with a heating rate of 10 °C min^{-1}. The weight loss by the sample was recorded and plotted against the temperature on the furnace. Moreover, from TGA software (Version 12, Mettler Toledo, Im Langacher, Greifensee, Switzerland, 2014), the derivative weight loss was automatically obtained.

The surface morphology and elemental component of the synthesized catalyst were determined via SEM JEOL, JSM6400 Scanning Electron microscopy (SEM, Petaling Jaya, Selangor, Malaysia) attached with Energy Dispersive X-ray Spectroscopy. Before analysis, the sample was dispersed on the aluminium stub sample holder and covered with silver tape. Then, the samples were dried overnight at 105 °C and subsequent gold coating using a sputter coater to prevent electric current induction. The gold coated sample was mounted onto the instrument for imaging and the voltage acceleration was set up to 12–20 kV. Different magnification of images was taken between 1000× to 10,000×. Moreover, the elemental analysis weight of carbon, oxygen, titanium, and sulphur on the surface of the catalyst was detected using EDX.

The nitrogen physisorption method was used to determine the textural properties of the synthesized catalysts using and an equipment Micro metrics analyser (Tristar II plus model, Petaling Jaya, Selangor, Malaysia). Prior to the determination, the sample was degassed for 8 h at 120 °C to remove any adsorbed molecules from the pores. Later, the Brunauer-Emmet-Teller (BET) surface area was measured at a relative pressure ranging from 0.04 to 0.4 where a linear relationship is maintained using the BET adsorption isotherm equation. While the Barret-Joyner-Halenda (BJH) method was used to calculate the pore volume and pore diameter of the samples from the desorption branch isotherm.

A Thermo Finnigan TPDRO series of NH_3-TPD coupled with thermos conductivity detector (TCD, Shah Alam, Selangor, Malaysia) was used to evaluate the distribution of acid sites and total acid density of the synthesized catalysts The principle of TPD involves pre-treatment, physisorption and chemisorption of the sample. In this work, 0.05 g samples were pre-heated to 150 °C for 1 h under Helium (He) gas with a flow rate of 20 mL min^{-1} to remove moisture and impurities in the sample. The adsorption of NH_3 gas occurred at room temperature for 30 min. Later, the sample was heated again with He gas at a heating rate of 10 °C min^{-1} for 5 min. Finally, the prepared sample was further heated to 950 °C with the carrier gas (He) and hold the temperature for another 5 min. TCD monitored and calculated the amount of NH_3 gas desorbed from the sample based on the integrated areas of the desorption peak throughout the heating process. Usually, the weakly bonded molecule (physisorption) is desorbed first followed by a strongly bounded molecule (chemisorption).

X-ray fluorescent (XRF), Shimadzu EDX-720 (Shimadzu Malaysia Sdn. Bhd., Petaling Jaya, Selangor, Malaysia) was used to determine the elemental composition of the sulphated and non-sulphated titania catalyst. About 0.5 g of synthesized catalyst was placed into a sample cup with a plastic support film. Then, the powder was pressed into a pallet form and placed in the instrument to run the analysis.

3.4. Glycerol Acetylation

The catalytic activity of the synthesized solid acid catalysts was performed in a glass batch reactor as shown in Figure 9. Prior to reaction, the 5SA catalyst was preheated to remove moisture. 5 g of glycerol and 0.5 g of 5SA catalyst (with respect to glycerol amount)

were weighed and added into 250 mL of a round bottom flask. 18.6 mL of acetic acid (with the ratio of 1:6 *w/v* of glycerol to acetic acid) was poured into the flask. A reflux condenser was fitted to the flask and the flask was immersed in a silicon oil bath. A magnetic bar was put into the mixture before the reaction starts. The reaction was carried out at 100–120 °C for 2–4 h under reflux conditions. The mixture was stirred under a constant stirring rate at 450 rpm. The procedures were repeated accordingly using 10SA, 15SA, 20SA, and TC catalysts. When the reaction was completed, the product was cooled and centrifuged at 3000 rpm for 10 min. The catalyst was separated using filter paper. The catalytic test was repeated without catalyst for blank reaction and denoted as TC.
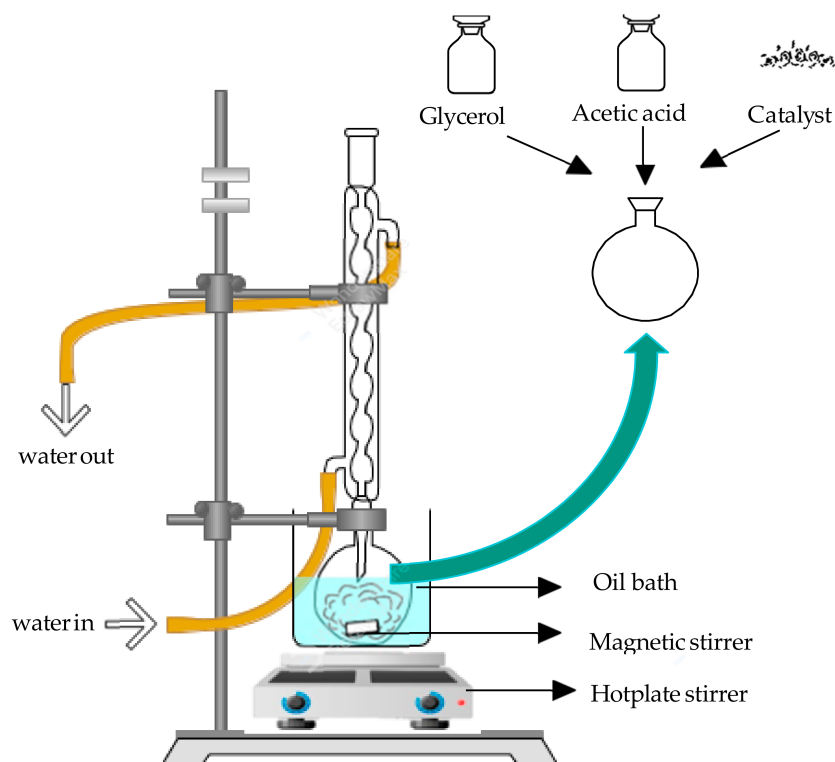
Figure 9. Experimental setup for glycerol acetylation using reflux condenser.

The obtained products (monoacetin, diacetin, and triacetin) were analysed using gas chromatography coupled with a flame ionized detector (GC-FID) (Agielent 7890A, Agielent Technologies Sales (Malaysia) Sdn. Bhd., Petaling Jaya, Selangor, Malaysia), FID, DB Wax 30 m × 0.25 mm ID × 0.25 μm). 1,3–butanediol and acetonitrile were used as internal standard and solvent, respectively. About 1 μL of the final sample was injected into the column initially set for 3 min at 80 °C. Then, heated again up to 260 °C with 10 °C min^{-1} and at 300 °C, the temperature ramping was increased to 30 °C min^{-1}. the area of the peak was used for the construction of the calibration curve and quantification analysis. The total time for GC-FID analysis was 22.3 min. The He gas was used as a carrier gas at a flow rate of 1.3 mL min^{-1}. The glycerol conversion (GL) and selectivity of MA, DA and TA can be calculated using the equation below [19,55]. These steps were repeated thrice to attribute error bars and statistical significance of the results.

$$\text{Equation for glycerol conversion } (\%): \frac{\text{Amount of glycerol converted}}{\text{Amount of glycerol feed}} \times 100$$

$$\text{Equation for selectivity } (\%): \frac{\text{Amount of specific product formed}}{\text{Total amount of product converted}} \times 100$$

4. Conclusions

The sulphated-titania catalyst was successfully prepared and tested on glycerol acetylation reaction. In this study, the concentration of sulphuric acid added into the titania play an important role in achieving the good properties favourable for glycerol acetylation. The catalyst acid properties and the surface porosity are crucial parts of catalytic activity. An increment in sulfuric acid concentration, reduces the surface area, pore volume, and particles size. However, the increment increased the number of active sites (Lewis acid) and strong acid strength. 15SA catalyst has high acid sites, strong acid strength, sufficient surface area and pore structure that contributes to the high conversion (90%) and highest TA selectivity (42%).

Author Contributions: Conceptualization, R.I.; Funding acquisition, R.I.; Methodology, M.R.S.F. and R.I.; Data curation, M.R.S.F.; Investigation, M.R.S.F. and N.S.; Project administration, I.N.S., R.I., S.L.L.; Supervision, R.I, Y.H.T.-Y., E.N.M.; Writing, M.R.S.F.; Writing, review and editing, I.N.S. and R.I. All authors have read and agreed to the published version of the manuscript.

Funding: This research was funded by Geran Penyelidikan Pembangunan Inovasi (GPPI/2019/9676400) and APC discount (700 CHF) was granted from MDPI Catalyst.

Acknowledgments: The authors deeply appreciate the GPPI grant (GPPI/2019/9676400) from Universiti Putra Malaysia, UTM-UPM CRG (Matching Grant/2019/9300458) and UTM Collaborative Research Grant (Cost centre: Q.J130000.2454.08G69). Catalysis Science and Technology Research Centre (PutraCat) is also gratefully acknowledged.

Conflicts of Interest: The authors hereby declare no conflict of interest.

References

1. Cannilla, C.; Bonura, G.; Maisano, S.; Frusteri, L.; Migliori, M.; Giordano, G.; Todaro, S.; Frusteri, F. Zeolite-assisted etherification of glycerol with butanol for biodiesel oxygenated additives production. *J. Energy Chem.* **2020**, *48*, 136–144. [CrossRef]
2. Arora, S.; Gosu, V.; Subbaramaiah, V.; Hameed, B.H. Lithium loaded coal fly ash as sustainable and effective catalyst for the synthesis of glycerol carbonate from glycerol. *J. Environ. Chem. Eng.* **2021**, *9*, 105999. [CrossRef]
3. Hu, C.; Yoshida, M.; Chen, H.C.; Tsunekawa, S.; Lin, Y.F.; Huang, J.H. Production of glycerol carbonate from carboxylation of glycerol with CO_2 using ZIF-67 as a catalyst. *Chem. Eng. Sci.* **2021**, *235*, 116451. [CrossRef]
4. Azri, N.; Irmawati, R.; Nda-Umar, U.I.; Saiman, M.I.; Taufiq-Yap, Y.H. Promotional effect of transition metals (Cu, Ni, Co, Fe, Zn)–supported on dolomite for hydrogenolysis of glycerol into 1,2-propanediol. *Arab. J. Chem.* **2021**, *14*, 103047. [CrossRef]
5. Raju, N.; Rekha, V.; Abhishek, B.; Kumar, P.M.; Sumana, C.; Lingaiah, N. Studies on continuous selective hydrogenolysis of glycerol over supported Cu-Co bimetallic catalysts. *New J. Chem.* **2020**, *44*, 3122–3128. [CrossRef]
6. Zhan, T.; Liu, W.; Teng, J.; Yue, C.; Li, D.; Wang, S.; Tan, H. Selective oxidation of glycerol to tartronic acid over Pt/N-doped mesoporous carbon with extra framework magnesium catalysts under base-free conditions. *Chem. Commun.* **2019**, *55*, 2620–2623. [CrossRef]
7. Katryniok, B.; Meléndez, R.; Bellière-Baca, V.; Rey, P.; Dumeignil, F.; Fatah, N.; Paul, S. Catalytic dehydration of glycerol to acrolein in a two-zone fluidized bed reactor. *Front. Chem.* **2019**, *7*, 127. [CrossRef]
8. Kansy, D.; Bosowska, K.; Czaja, K.; Poliwoda, A. The formation of glycerol oligomers with two new types of end groups in the presence of a homogeneous alkaline catalyst. *Polymers* **2019**, *11*, 144. [CrossRef]
9. Saengarun, C.; Petsom, A.; Tungasmita, D.N. Etherification of glycerol with propylene or 1-butene for fuel additives. *Sci. World J.* **2017**, *2017*, 4089036. [CrossRef]
10. Kulkarni, R.M.; Britto, P.J.; Narula, A.; Saqline, S.; Anand, D.; Bhagyalakshmi, C.; Herle, R.N. Kinetic studies on the synthesis of fuel additives from glycerol using CeO_2-ZrO_2 metal oxide catalyst. *Biofuel Res. J.* **2020**, *7*, 1100–1108. [CrossRef]
11. Aghbashlo, M.; Tabatabaei, M.; Rastegari, H.; Ghaziaskar, H.S. Exergy-based sustainability analysis of acetins synthesis through continuous esterification of glycerol in acetic acid using Amberlyst®36 as catalyst. *J. Clean. Prod.* **2018**, *183*, 1265–1275. [CrossRef]
12. Altino, F.M.R.S.; da Silva, D.S.; Bortoluzzi, J.H.; Meneghetti, S.M.P. Investigation of glycerol acetylation in the presence of Sb catalysts. *Biomass Convers. Biorefin.* **2021**, 1–10. [CrossRef]
13. Kumar, S.; Viswanadham, N.; Saxena, S.K.; Selvamani, A.; Diwakar, J.; Al-Muhtaseb, A.H. Single-pot template-free synthesis of a glycerol-derived C-Si-Zr mesoporous composite catalyst for fuel additive production. *New J. Chem.* **2020**, *44*, 8254–8263. [CrossRef]
14. Appaturi, J.N.; Jothi Ramalingam, R.; Selvaraj, M.; Chia, S.; Tan, S.H.; Khoerunnisa, F.; Ling, T.C.; Ng, E.P. Selective synthesis of triacetyl glyceride biofuel additive via acetylation of glycerol over NiO-supported TiO_2 catalyst enhanced by non-microwave instant heating. *Appl. Surf. Sci.* **2021**, *545*, 149017. [CrossRef]

15. Karnjanakom, S.; Maneechakr, P.; Samart, C.; Guan, G. Ultrasound-assisted acetylation of glycerol for triacetin production over green catalyst: A liquid biofuel candidate. *Energy Convers. Manag.* **2018**, *173*, 262–270. [CrossRef]

16. da Silva, D.S.; Altino, F.M.R.S.; Bortoluzzi, J.H.; Meneghetti, S.M.P. Investigation of Sn(IV) catalysts in glycerol acetylation. *Mol. Catal.* **2020**, *494*, 111130. [CrossRef]

17. Sun, J.; Tong, X.; Yu, L.; Wan, J. An efficient and sustainable production of triacetin from the acetylation of glycerol using magnetic solid acid catalysts under mild conditions. *Catal. Today* **2016**, *264*, 115–122. [CrossRef]

18. Silva, L.N.; Gonçalves, V.L.C.; Mota, C.J.A. Catalytic acetylation of glycerol with acetic anhydride. *Catal. Commun.* **2010**, *11*, 1036–1039. [CrossRef]

19. Reinoso, D.M.; Boldrini, D.E. Kinetic study of fuel bio-additive synthesis from glycerol esterification with acetic acid over acid polymeric resin as catalyst. *Fuel* **2020**, *264*, 116879. [CrossRef]

20. Carpegiani, J.A.; Godoy, W.M.; Guimarães, D.H.P.; Aguiar, L.G. Glycerol acetylation catalyzed by an acidic styrene-co-dimethacrylate resin: Experiments and kinetic modeling. *React. Kinet. Mech. Catal.* **2020**, *130*, 447–461. [CrossRef]

21. Mou, R.; Wang, X.; Wang, Z.; Zhang, D.; Yin, Z.; Lv, Y.; Wei, Z. Synthesis of fuel bioadditive by esterification of glycerol with acetic acid over hydrophobic polymer-based solid acid. *Fuel* **2021**, *302*, 121175. [CrossRef]

22. Dizoğlu, G.; Sert, E. Fuel additive synthesis by acetylation of glycerol using activated carbon/UiO-66 composite materials. *Fuel* **2020**, *281*, 118584. [CrossRef]

23. Tonutti, L.G.; Decolatti, H.P.; Querini, C.A.; Dalla Costa, B.O. Hierarchical H-ZSM-5 zeolite and sulfonic SBA-15: The properties of acidic H and behavior in acetylation and alkylation reactions. *Microporous. Mesoporous. Mater.* **2020**, *305*, 110284. [CrossRef]

24. Mertsoy, E.Y.; Sert, E.; Atalay, S.; Atalay, F.S. Fabrication of chromium based metal organic framework (MIL-101)/activated carbon composites for acetylation of glycerol. *J. Taiwan Inst. Chem. Eng.* **2021**, *120*, 93–105. [CrossRef]

25. Spataru, D.; Soares Dias, A.P.; Vieira Ferreira, L.F. Acetylation of biodiesel glycerin using glycerin and glucose derived catalysts. *J. Clean. Prod.* **2021**, *297*, 126686. [CrossRef]

26. Nda-Umar, U.I.; Ramli, I.B.; Muhamad, E.N.; Azri, N.; Amadi, U.F.; Taufiq-Yap, Y.H. Influence of heterogeneous catalysts and reaction parameters on the acetylation of glycerol to acetin: A review. *Appl. Sci.* **2020**, *10*, 7155. [CrossRef]

27. Cahyono, R.B.; Mufrodi, Z.; Hidayat, A.; Budiman, A. Acetylation of glycerol for triacetin production using Zr-natural zeolite catalyst. *ARPN J. Eng. Appl. Sci.* **2016**, *11*, 5194–5197.

28. Malaika, A.; Kozłowski, M. Glycerol conversion towards valuable fuel blending compounds with the assistance of SO_3H-functionalized carbon xerogels and spheres. *Fuel Process. Technol.* **2019**, *184*, 19–26. [CrossRef]

29. Banu, I.; Bumbac, G.; Bombos, D.; Velea, S.; Gălan, A.M.; Bozga, G. Glycerol acetylation with acetic acid over Purolite CT-275. Product yields and process kinetics. *Renew. Energy* **2020**, *148*, 548–557. [CrossRef]

30. Jiang, Y.; Li, X.; Zhao, H.; Hou, Z. Esterification of glycerol with acetic acid over SO_3H^- functionalized phenolic resin. *Fuel* **2019**, *255*, 115842. [CrossRef]

31. Magar, S.; Mohanraj, G.T.; Jana, S.K.; Rode, C.V. Synthesis and characterization of supported heteropoly acid: Efficient solid acid catalyst for glycerol esterification to produce biofuel additives. *Inorg. Nano-Metal Chem.* **2020**, *50*, 1157–1165. [CrossRef]

32. Beejapur, H.A.; La Parola, V.; Liotta, L.F.; Testa, M.L. Glycerol Acetylation over Organic-Inorganic Sulfonic or Phosphonic Silica Catalysts. *ChemistrySelect* **2017**, *2*, 4934–4941. [CrossRef]

33. Dalla Costa, B.O.; Decolatti, H.P.; Legnoverde, M.S.; Querini, C.A. Influence of acidic properties of different solid acid catalysts for glycerol acetylation. *Catal. Today* **2017**, *289*, 222–230. [CrossRef]

34. V Bokade, V. Synthesis of Oxygenated Fuel Additives via Acetylation of Bio-Glycerol over H_2SO_4 Modified Montmorillonite K10 Catalyst. *Prog. Petrochem. Sci.* **2018**, *1*, 1–5. [CrossRef]

35. Pradima, J.; Kulkarni, M.R. Archna Review on enzymatic synthesis of value added products of glycerol, a by-product derived from biodiesel production. *Resour. Technol.* **2017**, *3*, 394–405. [CrossRef]

36. Nda-Umar, U.I.; Ramli, I.; Muhamad, E.N.; Taufiq-Yap, Y.H.; Azri, N. Synthesis and characterization of sulfonated carbon catalysts derived from biomass waste and its evaluation in glycerol acetylation. *Biomass Convers. Biorefinery* **2020**, *40*, 437–446. [CrossRef]

37. Sudarsanam, P.; Peeters, E.; Makshina, E.V.; Parvulescu, V.I.; Sels, B.F. Advances in porous and nanoscale catalysts for viable biomass conversion. *Chem. Soc. Rev.* **2019**, *48*, 2366–2421. [CrossRef]

38. Almas, Q.; Sievers, C.; Jones, C.W. Role of themesopore generation method in structure, activity and stability of MFI catalysts in glycerol acetylation. *Appl. Catal. A Gen.* **2019**, *571*, 107–117. [CrossRef]

39. Jothi Ramalingam, R.; Radhika, T.; Adam, F.; Dolla, T.H. Acetylation of glycerol over bimetallic Ag–Cu doped rice husk silica based biomass catalyst for bio-fuel additives application. *Int. J. Ind. Chem.* **2016**, *7*, 187–194. [CrossRef]

40. Chipurici, P.; Vlaicu, A.; Calinescu, I.; Vinatoru, M.; Vasilescu, M.; Ignat, N.D.; Mason, T.J. Ultrasonic, hydrodynamic and microwave biodiesel synthesis – A comparative study for continuous process. *Ultrason. Sonochem.* **2019**, *57*, 38–47. [CrossRef] [PubMed]

41. Rane, S.A.; Pudi, S.M.; Biswas, P. Esterification of glycerol with acetic acid over highly active and stable alumina-based catalysts: A reaction kinetics study. *Chem. Biochem. Eng. Q.* **2016**, *30*, 33–45. [CrossRef]

42. Tomer, R.; Biswas, P. Dehydration of glucose/fructose to 5-hydroxymethylfurfural (5-HMF) over an easily recyclable sulfated titania (SO_4^{2-}/TiO_2) catalyst. *New J. Chem.* **2020**, *44*, 20734–20750. [CrossRef]

43. Geetha, S.; Thangamani, A.; Valliappan, R.; Vedanayaki, S.; Ganapathi, A. Sulfated titania (TiO$_2$-SO$_4^{2-}$) as an efficient and reusable solid acid catalyst for the multi-component synthesis of highly functionalized piperidines. *Chem. Data Collect.* **2020**, *30*, 100565. [CrossRef]

44. Patil, S.M.; Deshmukh, S.P.; More, K.V.; Shevale, V.B.; Mullani, S.B.; Dhodamani, A.G.; Delekar, S.D. Sulfated TiO$_2$/WO$_3$ nanocomposite: An efficient photocatalyst for degradation of Congo red and methyl red dyes under visible light irradiation. *Mater. Chem. Phys.* **2019**, *225*, 247–255. [CrossRef]

45. Gardy, J.; Hassanpour, A.; Lai, X.; Ahmed, M.H. Synthesis of Ti(SO$_4$)O solid acid nano-catalyst and its application for biodiesel production from used cooking oil. *Appl. Catal. A Gen.* **2016**, *527*, 81–95. [CrossRef]

46. Praveen, P.; Viruthagiri, G.; Mugundan, S.; Shanmugam, N. Structural, optical and morphological analyses of pristine titanium di-oxide nanoparticles - Synthesized via sol-gel route. *Spectrochim. Acta-Part A Mol. Biomol. Spectrosc.* **2014**, *117*, 622–629. [CrossRef]

47. Nachit, W.; Touhtouh, S.; Ramzi, Z.; Zbair, M.; Eddiai, A.; Rguiti, M.; Bouchikhi, A.; Hajjaji, A.; Benkhouja, K. Synthesis of nanosized TiO$_2$ powder by sol gel method at low temperature. *Mol. Cryst. Liq. Cryst.* **2016**, *627*, 170–175. [CrossRef]

48. Humelnicu, A.C.; Samoila, P.; Asandulesa, M.; Cojocaru, C.; Bele, A.; Marinoiu, A.T.; Sacca, A.; Harabagiu, V. Chitosan-sulfated titania composite membranes with potential applications in fuel cell: Influence of cross-linker nature. *Polymers* **2020**, *12*, 1125. [CrossRef]

49. Dabbawala, A.A.; Alhassan, S.M.; Mishra, D.K.; Jegal, J.; Hwang, J.S. Solvent free cyclodehydration of sorbitol to isosorbide over mesoporous sulfated titania with enhanced catalytic performance. *Mol. Catal.* **2018**, *454*, 77–86. [CrossRef]

50. Yang, W.; Ok, Y.S.; Dou, X.; Zhang, Y.; Yang, M.; Wei, D.; Xu, P. Effectively remediating spiramycin from production wastewater through hydrolyzing its functional groups using solid superacid TiO$_2$/SO$_4$. *Environ. Res.* **2019**, *175*, 393–401. [CrossRef]

51. de Oliveira, C.R.S.; Batistella, M.A.; Ulson de Souza, A.A.; Ulson de Souza, S.M.d.A.G. Synthesis of superacid sulfated TiO$_2$ prepared by sol-gel method and its use as a titania precursor in obtaining a kaolinite/TiO$_2$ nano-hybrid composite. *Powder Technol.* **2021**, *381*, 366–380. [CrossRef]

52. Deris, N.H.; Rashid, U.; Soltani, S.; Choong, T.S.Y.; Nehdi, I.A. Study the effect of various sulfonation methods on catalytic activity of carbohydrate-derived catalysts for ester production. *Catalysts* **2020**, *10*, 638. [CrossRef]

53. Liu, G.; Tsen, W.C.; Hu, F.; Zhong, F.; Wang, J.; Liu, H.; Wen, S.; Zheng, G.; Qin, C.; Gong, C. Enhanced proton conductivities of chitosan-based membranes by inorganic solid superacid SO$_4^{2-}$–TiO$_2$ coated carbon nanotubes. *Int. J. Hydrogen Energy* **2020**, *45*, 29212–29221. [CrossRef]

54. Reddy, P.S.; Sudarsanam, P.; Raju, G.; Reddy, B.M. Synthesis of bio-additives: Acetylation of glycerol over zirconia-based solid acid catalysts. *Catal. Commun.* **2010**, *11*, 1224–1228. [CrossRef]

55. Nda-Umar, U.I.; Irmawati, R.; Muhamad, E.N.; Azri, N.; Ishak, N.S.; Yahaya, M.; Taufiq-Yap, Y.H. Organosulfonic acid-functionalized biomass-derived carbon as a catalyst for glycerol acetylation and optimization studies via response surface methodology. *J. Taiwan Inst. Chem. Eng.* **2021**, *118*, 355–370. [CrossRef]